

STUDY OF LOCAL STRESS STATE AND FRETTING PARAMETERS IN A SPHERE-PLAN CONTACT UNDER FRETTING FATIGUE CONDITIONS

Patrícia Rocha Maia

Luiz Carlos Rolim Lopes

Universidade Federal Fluminense, Escola de Engenharia Industrial Metalúrgica de Volta Redonda, Avenida dos Trabalhadores, 420, Vila Santa Cecília, Volta Redonda, RJ-Brazil.

rm.patricia@gmail.com, rolimlop@metal.eeimvr.uff.br

Abstract. Fretting problems occur in components submitted to contact loading and relative displacement induced by cyclic loading. The contact is submitted to micro-displacements, severe tri-axial stress state and plastic strain accelerating damage accumulation and causing premature fail. Prediction of failure is a difficult task, due to the complexity of the contact phenomena and the various factors that cause damage accumulation. Besides, in the experimental physical models the measurement of the parameters in the contact is performed indirectly. Thus, in this work a numerical model was built and fretting fatigue simulations were performed to study the local stress state in a sphere-plan contact region using ABAQUS application. The model considered a normal force applied to a spherical base pin over a specimen submitted to cyclic stress amplitude, both parts constructed with RQC-100 steel. The results have shown slip amplitude variations with different normal forces and cyclic stresses. For constant normal force, the tangential force increases with decreasing cyclic stress. The local plastic strain as a function of cyclic stress and normal force variations were discussed. Dissipated energy increases with increasing normal force and is insensitive to low cyclic stress. This study can be applied in the design of different parts found in mobility and other engineering systems such as bolted and riveted joints; flanged joints; turbine blades.

Keywords: fretting fatigue, finite element method, micro-displacement local plastic strain, local tangential force.

1. INTRODUCTION

The phenomenon of fretting has been recognized for over a century. Fretting problems occur in contact region of components submitted to contact loading and relative displacement induced by cyclic loading. The contact region is submitted to micro-displacements, severe tri-axial stress state and local plastic strain whose accelerate damage accumulation and cause premature fail by crack nucleation and propagation. Under fretting conditions, fatigue strength can be reduced by 50 to 70%, relative to plain fatigue (Hills and Nowell, 1994; Forsyth, 1981). Recently, Nowell et al. (2006) presented a review on experimental investigations of fretting fatigue performed on different devices and load configurations. These investigations provided focus on fretting problems in various engineering fields, for example: aerospace, automobile, nuclear sectors (Altenberger et al., 2002; Nowell, 2000; Fouvry et al., 2003; Jedrzejczyk et al., 2009; Helmi Attia, 2006). These studies encompass dovetail joint in an engine, ball bearings, bolted and rivet joints, pin-held fixtures that are subjected to oscillatory loading. Other mechanical systems of also with great importance, suffer with component failures due to fretting fatigue. Some examples of these systems are trains, cars, trucks, buses, steel cables and orthopedic implants. (Hin, 2004).

Prediction of failure is a difficult task, due to the complexity of the contact phenomena and the various factors that cause damage accumulation. Besides, in the experimental physical models the measurement of the parameters in the contact is performed indirectly, due to the difficulty of access to the site. In a simple geometry of a fatigue specimen under fretting conditions, the important parameters for stress analysis are the normal force, F_n , the tangential force, Q and specimen cyclic stress, σ_c that can be predicted (Popov, 2010) as shown in Fig. 1.

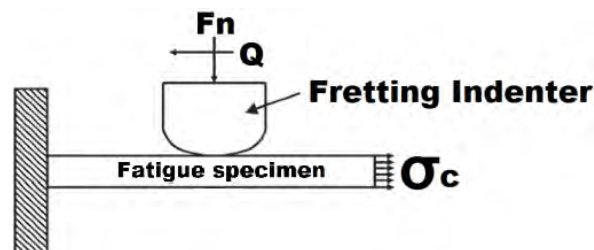


Figure 1. Fatigue specimen, fretting indenter fretting parameters, normal contact force, F_n , tangential force, Q , and cyclic stress, σ_c .

The fretting cycle can be analyzed, as a plot of dissipated energy as a function of slip amplitude, as shown in Fig. 2.

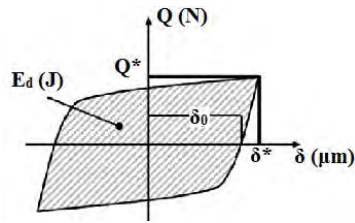


Figure 2. Fretting cycles and its parameters: slip amplitude, δ_0 , tangential force, Q , and dissipated energy, E_d .

Were δ^* is the maximum slip amplitude, Q^* is the maximum tangential force, J is the unit of dissipated energy, Joules. Q Vingsbo and Söderberg (1988) relate the fatigue life to the slip amplitude, as shown in the Fig. 3. The fatigue life decreases with increasing slip amplitude up to a certain value of slip amplitude. And then, for further increasing in slip amplitude, the fatigue life increases.

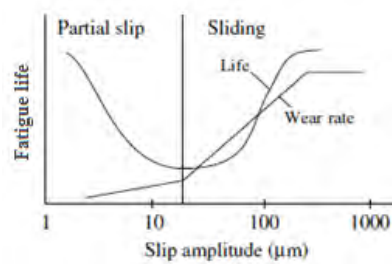


Figure 3. Schematic diagram of the variation of fretting fatigue life and fretting wear rate with slip amplitude (Vingsbo and Söderberg, 1988).

The energy ratio is the ration between dissipated energy, E_d , and the total energy, E_t , and can be analyzed from the fretting cycle plot, see Fig. 4 (Fouvry et al, 1995). The criterion for determining the transition between partial and total slip regimes is given by the energy ratio, A :

$$A = \frac{E_d}{E_t} \quad (1)$$

The total energy E_t is expressed as:

$$E_t = 4Q^*\delta^* \quad (2)$$

The transition occurs for the critical value of $A_t = 0.2$. So, if $A < A_t$, the contact is subjected to partial slip regime, and if $A \geq A_t$, it is subjected to total slip regime.

The energy ratio, A , is considered independent on the material properties, the geometry of the parts in contact and the coefficient of friction (μ).

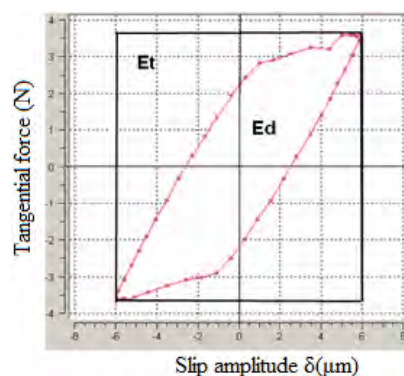


Figure 4. Total energy and dissipated energy (Perrinet, 2009)

From another point of view, the transition from partial to total slip regime of fretting can be analyzed from a plot of tangential force versus displacement, as shown in Fig. 5 (Perrinet, 2009). For low displacements combined with a low tangential force, the contact is in partial slip regime. Similarly, large displacements associated to high tangential forces indicate total slip regime.

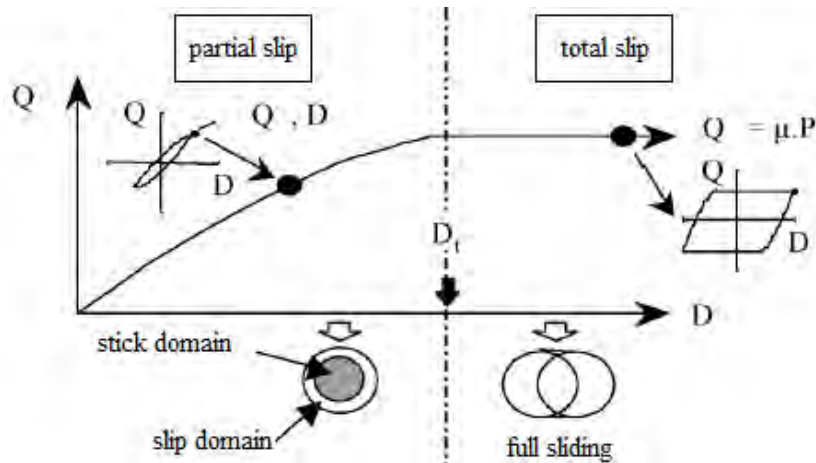


Figure 5. Total slip and partial slip for a sphere-plan contact, where D is slip amplitude.

However, analytical solutions employing linear elastic mechanics do not allow an approach of the actual stress state in the contact region, since the friction problems and plasticity at the contact interface produce nonlinearities which modify the stress and strain distributions. Furthermore, the use of analytical solutions may become complex if considering nonlinearities. Thus, the use of numerical tool for studying fretting problems can bring about significant contribution to the understanding of the stress state developed in the region of contact in complement to the results obtained from physical models. Also, it allows for greater reliability in predicting the performance of components subject to fretting fatigue.

With the aim of predicting strength and life under fretting conditions, different works on numerical modelling and simulation have been done and published recently, for examples see the following references: Barnabé Filho (2003); Ding et al. (2004); Hirsch and Neu, (2011); Proudhon and Basseville (2011). Great part of the works has considered the cylindrical-plan geometry. In this work a numerical model was built and fretting fatigue simulations were performed to study the local stress state in a sphere-plan contact geometry using ABAQUS application (Hibbitt et al., 2009). The model considered a normal contact force applied to a spherical base pin over a specimen submitted to cyclic stress amplitude, both parts constructed with RQC 100 steel (Stephens, 2001). Fretting parameters as normal pressure on the indenter and cyclic stress amplitude acting on the specimen are imposed as variables. The effects of normal force and cyclic stress on local slip amplitude, tangential force, plastic strain, and dissipated energy in the contact were analyzed.

2. METHODOLOGY

2.1 The model formulation

The model consists of a fatigue sample over which an indenter with spherical extremity is in contact by the action of a normal force. The idealized model is shown in Fig. 6 and provides a hertzian sphere-plan contact (Johnson, 1985).

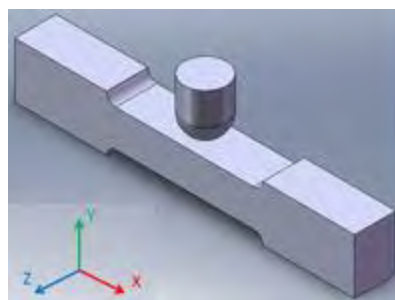


Figure 6. Idealized model of a sphere-plan contact.

The FEM (Finite Element Method) was built using ABAQUS application. The indenter has a radius of 2.3 mm and the fatigue specimen has the following dimensions: Length: 2 mm x Width: 2 mm x Height: 0.5 mm. The FEM analysis has been performed in the surroundings of the contact region. For the indenter it was chosen the tetrahedral element in a 3-D mesh of 70 μm . For the fatigue sample the 3-D mesh is composed of hexahedral elements of 15 μm . The stress and strain analyses were carried out on the fatigue specimen. The boundary conditions was as follows: (i) restriction to displacement in y and z directions imposed to lower face of the fatigue specimen, so that it can only has move on x direction; (ii) the fatigue specimen is clamped in left shoulder and a cyclic stress is applied to its right shoulder; (iii) restriction of displacement in x and z directions imposed to the indenter, so that it can only move on y direction; (iv) the normal contact force is applied to the indenter in a homogeneous distributed way over an its hemispheric section; (v) the components of the model were built with a z plan symmetry. Figure 7 shows the model with the imposed boundary conditions.

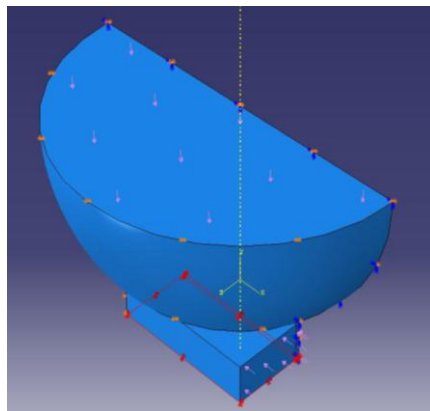


Figure 7. Boundary conditions.

2.2 The material

The used material was the RQC-100 steel both for the indenter and specimen. The input data for mechanical properties were introduced via the cyclic stress-strain curve of this steel, shown in Fig.8 (Stephens, 2001). The cyclic stress-strain curve was preferred to the tensile stress-strain curve in order to take in to consider the cyclic softening behavior of the RQC-100 steel for loading near its yield strength. As can be observed from the curve, the cyclic yield strength, σ_y , for this material is around 650 MPa.

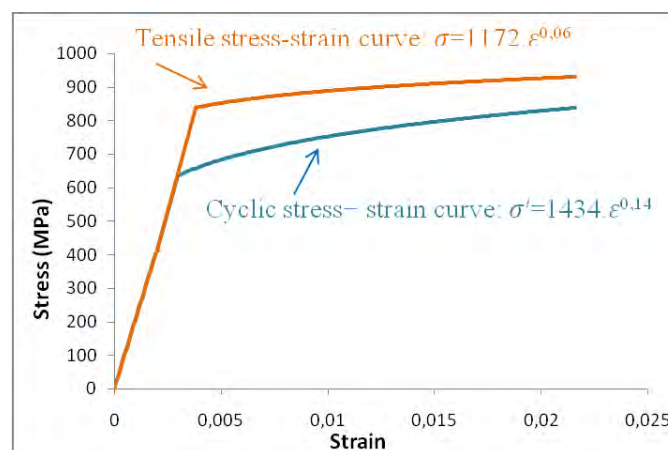


Figure 8. Stress-strain curves for RQC-100 steel.

2.3 The fretting simulations

For analysis of the effect of stress concentration, the applications of normal force and cyclic stresses in modeling were performed according to Tab. 1. These values of cyclic load were set considering the cyclic curve of material, as 55% and 77% of its cyclic yield strength (650 MPa).

Table 1. Cyclic stress and normal force used in the simulation.

Cyclic stress – σ_a (MPa)	360				430				500			
Normal Force – F_n (N)	0.5	1	2	4	0.5	1	2	4	0.5	1	2	4

From the simulations it was taken as output data the tangential force, the contact pressure, the displacement in the contact region, plastic strain under the indenter. The dissipated energy in the contact region was measure through the area under the tangential force versus displacement plot using the AUTOCAD application (Autodesk Inc., 2006).

3. RESULTS AND DISCUSSIONS

3.1 Effect of cyclic stress and normal contact force on fretting slip

Figure 9 shows that for lower cyclic stress amplitude: 360 MPa and 430 MPa (55% and 66% of σ_y respectively), slip amplitude, δ_0 , decreases with increasing normal contact force. For higher cyclic stress amplitude, 500 MPa (approximately close to 77% of σ_y), an increase in the slip amplitude is observed with increasing normal contact force, for contact force higher than 1 N.

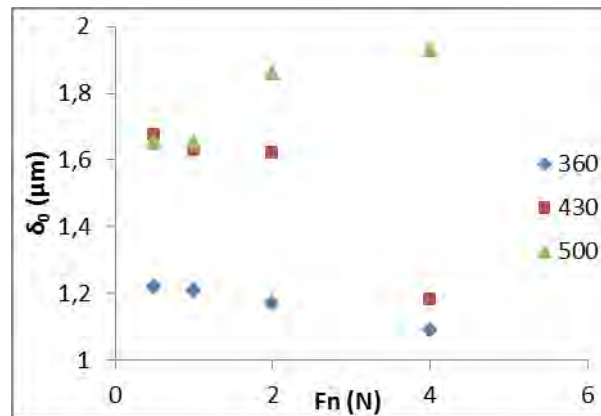


Figure 9. Slip amplitude as a function of normal force.

From another point of view, Fig.10 shows that for lower cyclic stresses (360, 430 MPa) slip amplitude decreases with increasing contact normal force, F_n . Thus, F_n is effective in increasing fatigue life, since as seen in Fig. 3, fretting fatigue life increases when slip amplitude decreases. However, for higher cyclic stress (500 MPa), the opposite condition is observed. So, for severe cyclic loading, increasing F_n brings no benefits to fretting fatigue life.

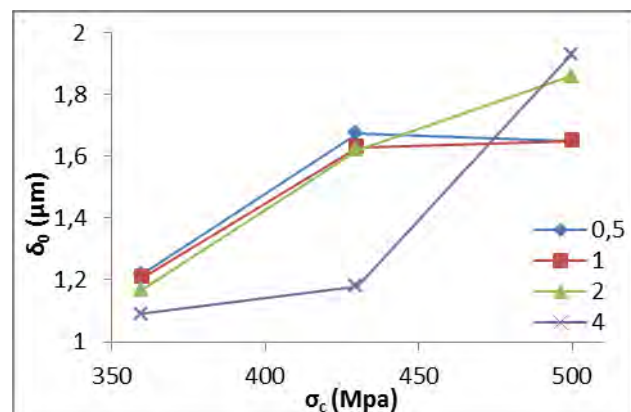


Figure 10. Slip amplitude as a function of cyclic stress, for different values of normal contact force.

3.2 Effect of normal force on tangential force

Figure 11 presents the variation of tangential force, Q^* , with cyclic stress amplitude, σ_c for different normal contact forces. It can be observed that tangential force decreases with increasing cyclic stress, for a given normal contact force. For a given cyclic stress, the tangential force increases with increasing the normal force. The effect of normal contact force on tangential force with is greater if compared to the effect of the cyclic stress variation, as can be seen in Tab. 2:

$$\left. \frac{\partial(Q^*)}{\partial F_n} \right|_{\sigma_c} > \left. \frac{\partial(Q^*)}{\partial \sigma_c} \right|_{F_n} \quad (3)$$

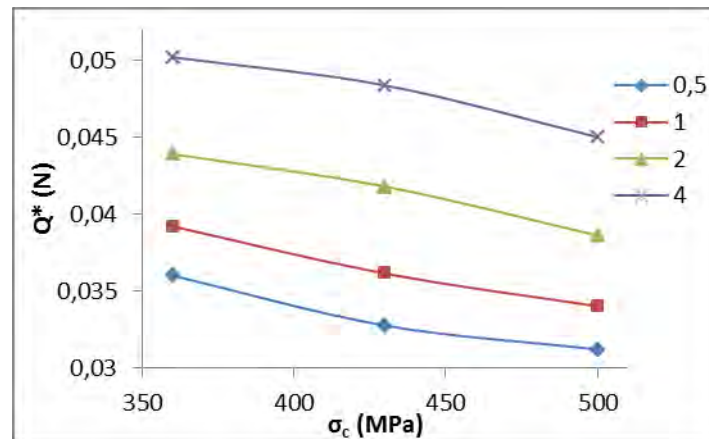


Figure 11. Relationship between normal force, tangential force and cyclic stress amplitude.

Table 2. Effect on tangential force, Q^* : (a) of normal contact force, F_n , for constant σ_c , and (b) of cyclic stress, σ_c , for constant F_n .

		Tangential Force (N)			(b) $\delta(Q^*)/\delta\sigma_c$ constant F_n
σ_y (Mpa)		360	430	500	
F_n (N)	0,5	0,036000	0,032748	0,031200	0,0048
	1	0,039200	0,036126	0,034000	0,0052
	2	0,043900	0,041786	0,038600	0,0053
	4	0,050200	0,048371	0,045000	0,0052
(a) $\delta(Q^*)/\delta F_n$ for constant σ_c		0,0142	0,0142	0,0138	-

3.3 Effect of cyclic stress and normal contact force on local plastic strain

From Fig. 12, it is observed that the effect of cyclic stress on the plastic strain, ϵ_p , is small if compared to the effect of the normal contact force. As seen in Tab. 3:

$$\left. \frac{\partial(\epsilon_p)}{\partial(F_n)} \right|_{\sigma_c} > \left. \frac{\partial(\epsilon_p)}{\partial(\sigma_c)} \right|_{F_n} \quad (4)$$

Inside the contact area, the material is under a severe multiaxial stress state in an analogy to notched region. So, the material under the indenter is subjected to non-proportional loading. The local plastic strain is higher than the offset strain value of 0.2% and it seems that the cyclic stress does not affect the plastic strain considerably. Thus, the plastic strain depends strongly on contact normal force. However, the effect of cyclic stress is enhanced by higher normal force (4N).

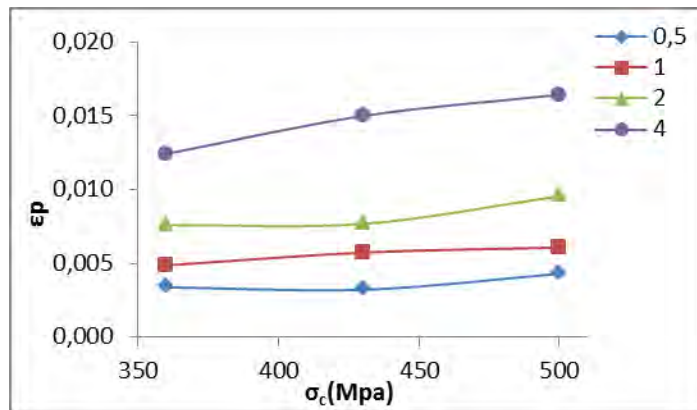


Figure 12. Effect of cyclic stress, σ_c , and contact normal force, F_n , on plastic strain in the contact area.

Table 3. Effect on local plastic strain, ϵ_p of: (a) normal contact force, F_n , for constant σ_c , and (b) cyclic stress, σ_c , for constant normal contact force, F_n .

Local Plastic Strain (ϵ_p)				(b) $\delta(\epsilon_p)/\delta\sigma_c$ constant F_n	
σ_y (Mpa)	360	430	500		
F_n (N)	0,5	0,003384	0,0032159	0,0043009	0,00091714
	1	0,004868	0,0057354	0,0060787	0,00121063
	2	0,007600	0,0076816	0,0095587	0,00195899
	4	0,012432	0,0149956	0,0164367	0,0040048
(a) $\delta(\epsilon_p)/\delta F_n$ constant σ_c		0,0090482	0,0117797	0,0121358	-

3.4 Effect of cyclic stress and normal contact force on dissipated energy

Figure 13 shows that fretting dissipated energy increases with increasing normal contact force and is nearly independent on the cyclic stress for cyclic stress up to 430 MPa. For cyclic stress higher than 430 MPa, the dissipated energy increases with cyclic stress being potentiated by greater normal contact forces (2 N and 4 N), as seen in Tab. 4:

$$\left. \frac{\partial(E_d)}{\partial\sigma_c} \right|_{F_n, \sigma_c > 430} > \left. \frac{\partial(E_d)}{\partial\sigma_c} \right|_{F_n, \sigma_c < 430} \tag{5}$$

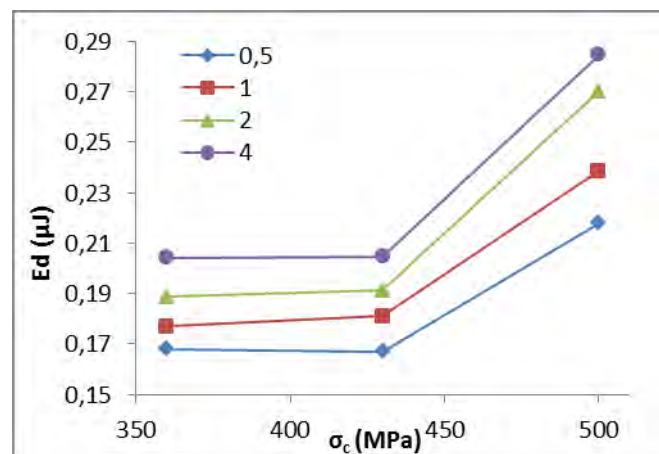


Figure 13. Dissipated energy as a function of cyclic stress.

Table 4. Effect on dissipated energy, E_d , of (a) F_n , to σ_c constant, and dissipated energy over σ_c , to constant F_n , in different regions of the curves.

Dissipated Energy, E_d (μJ)				(b) $\delta(E_d)/\delta\sigma_c$ [430-360 MPa] constant F_n	(b) $\delta(E_d)/\delta\sigma_c$ [500-430 MPa] constant F_n	
σ_y (Mpa)	360	430	500			
F_n (N)	0,5	0,16811	0,16700	0,21789	0,00111	0,05089
	1	0,17687	0,18108	0,23849	0,00421	0,05741
	2	0,18864	0,19127	0,27008	0,00263	0,07881
	4	0,20422	0,20466	0,28468	0,00044	0,08002
(a) $\delta(E_d)/\delta F_n$ constant σ_c		0,03611	0,03766	0,06679	-	-

3.5 Fretting cycles

According to the energy ratio described by Fouvry et al. (1995), to lower ratio of dissipated energy E_d and the total energy E_t , the system tends to the behavior of partial slip. To higher ratio, the system tends to the behavior of total slip.

Changing the normal force, to constant cyclic stress of 360MPa, we have the following fretting cycles in Fig. 14:

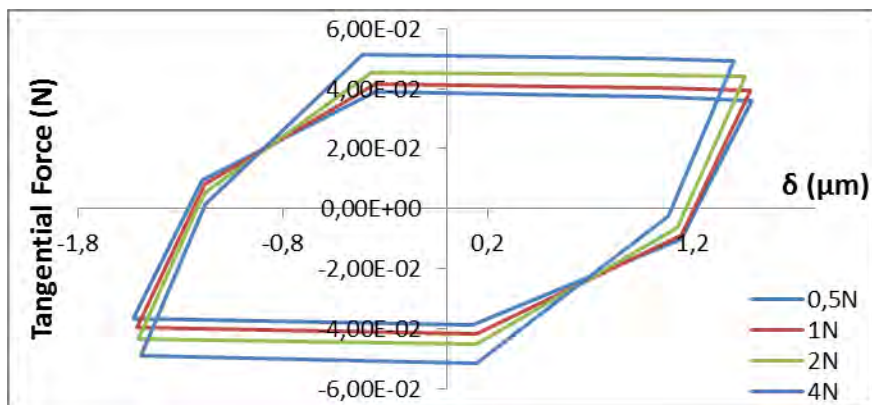


Figure 14. Fretting cycles of each normal force, with constant cyclic stress of 360MPa.

These fretting cycles allow the calculation of both total and dissipated energy for variation of each normal force (Tab. 5).

Table 5. Energy ratio to each normal force, to constant cyclic stress of 300 MPa.

Normal Force F_n (N)	0,5	1	2	4
Dissipated Energy E_d (μJ)	0,16811	0,17687	0,18864	0,20422
Total Energy E_t (μJ)	0,23429	0,24938	0,26819	0,29723
Energy Ratio (E_d/E_t)	0,71753	0,70924	0,70338	0,68708

As we can see to the normal force of 0.5 N, the characteristics of fretting cycle tends to total slip regime, shown by the higher slip magnitude (δ_0) and also shown by the higher value of the energy ratio (Tab. 5), which confirms the total slip behavior observed for this normal force.

Increasing the normal force, it is noticed a tendency to approach the fretting cycle to partial slip configuration shown in Fig. 5. In other words, with the decrease of the dissipated energy (E_d), the energy ratio obviously falls, confirming the observation that increasing the normal force, the system tends to partial slip regime in low cyclic stresses.

For normal force of 4N, there is a decrease in the slip amplitude (δ_0) and also in Fig. 14 and in Tab. 5 is shown the lower energy ratio, i.e., a tendency to partial slip state characterized by cycle more closed.

Changing the normal force, to constant cyclic stress of 430MPa, we have the following fretting cycles in Fig. 15:

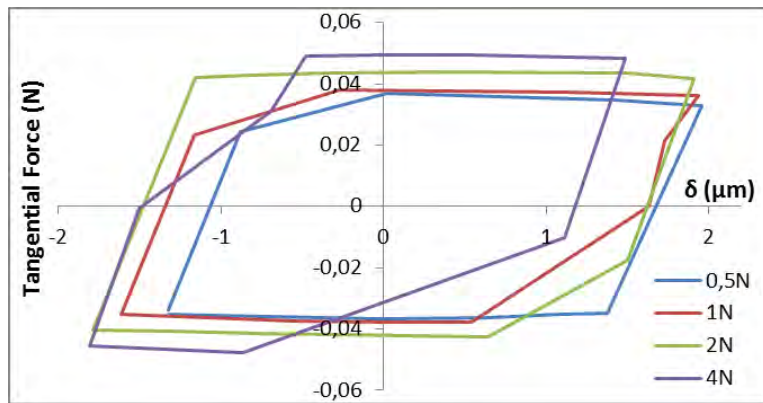


Figure 15. Fretting cycles of each normal force, with constant cyclic stress of 430MPa.

These fretting cycles allow the calculation of both total and dissipated energy for variation of each normal force (Tab. 6).

Table 6. Energy ratio to each normal force, to constant cyclic stress of 430 MPa.

Normal Force F_n (N)	0,5	1	2	4
Dissipated Energy E_d (μ J)	0,167	0,18108	0,19127	0,20466
Total Energy E_t (μ J)	0,24158	0,24791	0,2587	0,32003
Energy Ratio (E_d/E_t)	0,69128	0,73043	0,7394	0,6395

According to Fig. 15, we also observe decrease in slip amplitude and increase in dissipated energy with increasing normal force, but the energy ratio cannot be related to the variation of normal force, as noted in Fig. 17 below, the energy ratio suffers greater influence from cyclic stress.

Changing the normal force, to constant cyclic stress of 500MPa, we have the following fretting cycles in Fig. 16:

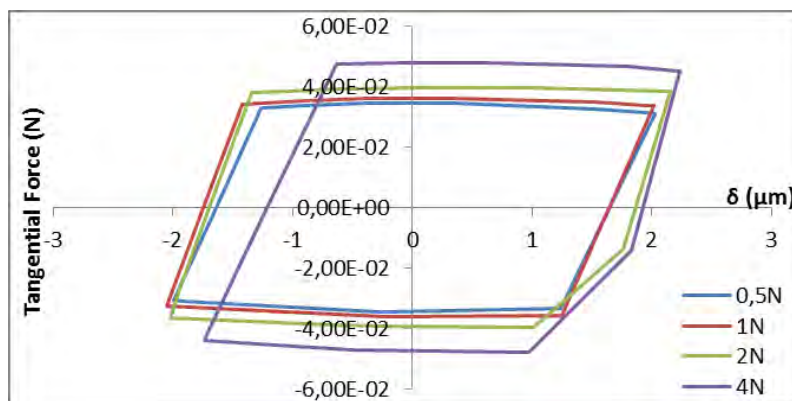


Figure 16. Fretting cycles of each normal force, with constant cyclic stress of 500MPa.

These fretting cycles allow the calculation of both total and dissipated energy for variation of each normal force (Tab. 7).

Table 7. Energy ratio to each normal force, to constant cyclic stress of 500 MPa.

Normal force F_n (N)	0,5	1	2	4
Dissipated Energy E_d (μ J)	0,21789	0,23849	0,27008	0,28468
Total Energy E_t (μ J)	0,27351	0,29455	0,33139	0,38106
Energy Ratio (E_d/E_t)	0,79664	0,80968	0,81499	0,74707

3.6 Energy ratio

Figure 17 shows energy ratio varying with increasing normal force to each cyclic stress. Observing the figure in the direction of increasing cyclic stress, it is seen that the energy ratio increases. This is due to the fact that to higher cyclic stress, the relative movement between the components increase, this movement also represented when fretting cycle tends to open (higher energy dissipation due to the increase of the relative movement).

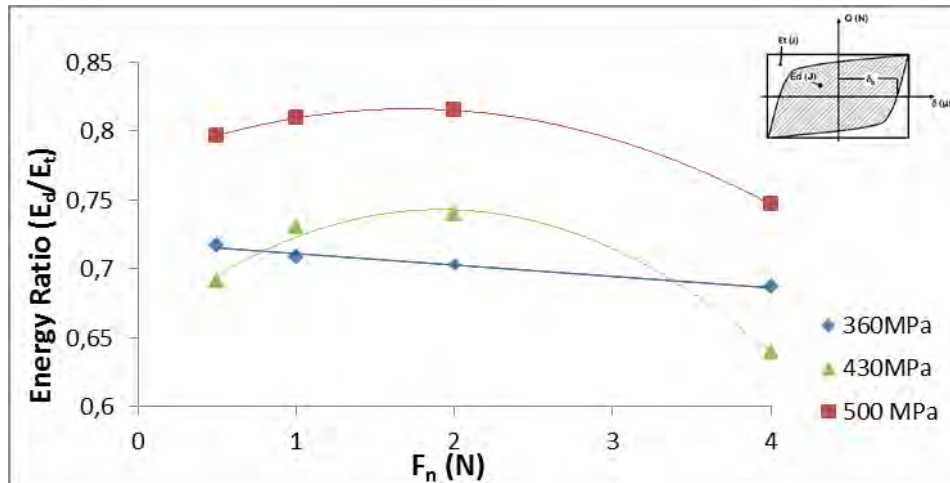


Figure 17. Energy ratio to each normal force.

To 360MPa of cyclic stress, there is a decrease in the energy ratio when increasing the pressure on the pin, i.e., increasing the normal force, there is a tendency of partial slip behavior, with the existence of a zone of adhesion. However decreasing normal force, there is a tendency to total slip regime without zone of adhesion.

It is observed that normal forces smaller than 2N, to 500MPa to 430MPa of cyclic stress, does not conform to the observed behavior of cyclic stress of 360MPa. This is due to high cyclic stress applied to the specimen, these values being very close to the cyclic yield strength of the material. However the fretting cycle to the normal force of 4N is represented according to the behavior observed for 360MPa, because the normal force of 4N already have a relatively great enough to cause adherence of the contact area under high cyclic load.

3.7 Relationship between tangential force and contact pressure

Figure 18 shows that when cyclic stress increases it is observed a decrease in the maximum tangential force, Q^* . This maximum tangential force is the contact resistance to the movement generated by the cyclic stress, so we conclude that with increasing cyclic stress, the resistance to movement decreases.

Analysis of growth in the direction of the normal force (0.5N to 4N), we observe that not only the maximum pressure increases, as also the resistance to movement. This shows that the increase in pressure on the pin tends to prevent or reduce slip between the components to low cyclic stresses.

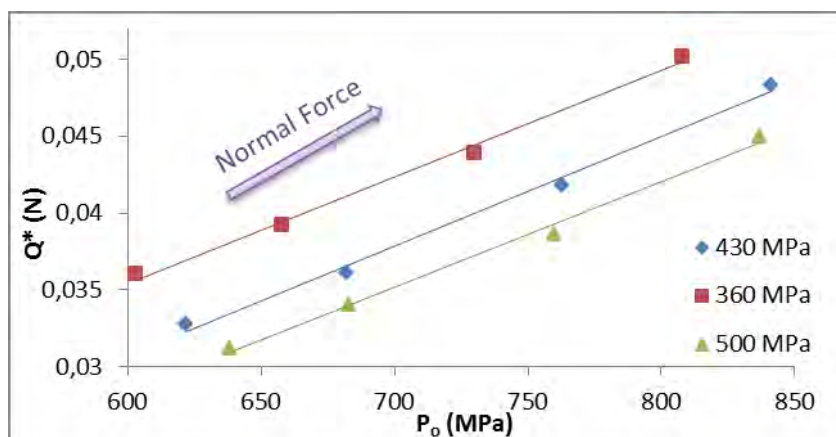


Figure 18. Maximum tangential force as a function of maximum pressure.

4. CONCLUSIONS

In this work, a numerical model of a flat fatigue specimen submitted to different reversed cyclic stress amplitudes and under the action of different normal contact forces on a spherical indenter was built using the ABAQUS application and its fretting fatigue stress state has been simulated and analyzed.

Important parameters of fretting fatigue process such as: slip amplitude, dissipated energy, tangential load and also local plastic strain have been analyzed from fretting simulations.

Local plastic strain and tangential force are affected strongly by normal force, and secondarily by cyclic stress. The effect of cyclic stress on local plastic strain is enhanced by higher normal force.

Dissipated energy is nearly independent on the cyclic stress for lower cyclic stresses, but it increases with increasing normal force for all cyclic stresses studied. For higher cyclic stress, the increasing of dissipated energy is potentiated to higher normal force.

The energy ratio increases with increasing cyclic stress, also observed by the tendency to the fretting cycle to enlarge. For low cyclic stress the energy ratio decreases with increasing normal force, however for high cyclic stress, this is not observed because the values come close to the cyclic yield strength of the material.

It was observed that for lower cyclic stresses, slip amplitude decreases with increasing normal contact force, so that increasing normal contact force is an effective way of increasing fretting fatigue life. However, for high cyclic stress the opposite is observed.

5. REFERENCES

- Altenberger, I., Nalla, R. K., Noster, U. et al., 2002. "On the Fatigue Behavior and Associated Effect of Residual Stresses in Deep-Rolled and Laser Shock Peened Ti-6Al-4V Alloys at Ambient and Elevated Temperatures". In *Seventh National Turbine Engine High Cycle Fatigue (HCF) Conference*, C. Burns, ed., Universal Technology Corp., Dayton, OH.
- Abaqus 6.9, 2009. Hibbitt, Karlsson & Sorensen, Inc., Pawtucket, RI, USA.
- AutoCAD 2006 Release 16.2, Autodesk Inc, State of California, USA.
- Barnabé Filho, S., 2003. *Simulação de um Ensaio de Fadiga por Fretting Empregando o Método dos Elementos Finitos*. Masters dissertation, Escola de Engenharia Industrial Metalúrgica de Volta Redonda, Universidade Federal Fluminense, Rio de Janeiro.
- Ding, J., Leen, S.B., McColl, I.R., "International Journal of Fatigue", 26, 521-531, 2004.
- Forsyth, J.E., "Occurrence of Fretting Fatigue Failures in Practice", Ed. R.B. Waterhouse, *Fretting Fatigue*, Applied Science Publisher LTD, 1981, pp.99-125.
- Fouvry, S., Kapsa, Ph., Vincent, L., 2003. *Fretting Fatigue: Advances in Basic Understanding and Applications*, ASTMSTP1425, Y. Mutoh, S. E. Kinyon, and D. W. Hoepfner ed., ASTM International, West Conshohocken, PA.
- Fouvry, S., Kapsa, Ph., Vincent, L., 1995 "Analysis of Sliding Behaviour for Fretting Loadings: Determination of Transition Criteria", In *Wear* 185 3546.
- Helmi Attia, M., 2006. "Fretting Fatigue and Wear Damage of Structural Components in Nuclear Power Station – Fitness for Service and Life Management Perspective", In *Tribology International* 39.
- Hills, D.A., Nowell, D., 1994. *Mechanics of Fretting Fatigue*, Kluwer Academic Publishers, Oxford, UK.
- Hin T., S., Sumita M., 2004. *Engineering Materials for Biomedical Applications*, World Scientific Publishing Ed. .
- Hirsch, M.R., Neu, R.W., 2011. "Fretting Damage in Thin Sheets: Analysis of an Experimental Configuration", In *Tribology International* 44, 1503-1510.
- Jedrzejczyk, P., Chad, S., Fouvry, S., Chalandon, P., 2009. "Impact of the Nickel Interlayer on the Electrical Resistance of Tin-tin Interface Submitted to Fretting Loading", In *Surface and Coating Technology* 203.
- Johnson, K.L., 1985. *Contact Mechanics*, Cambridge University Press, Cambridge. Apud I.R. McColl, J. Ding, S.B. Leen, 2004. "Finite Element Simulation and Experimental Validation of Fretting Wear". In *Wear* 256 1114–1127.
- Nowell, D., 2000. *Progress in Structural Mechanics*, J. Morton and F. Paris, University of Seville; ISBN 8488783450: 61-72.
- Nowell, D., Dini, D., Hills, D.A., 2006. "Recent Developments in the Understanding of Fretting Fatigue", In *Engineering Fracture Mechanics*, 73, 207-222.
- Perrinet, O., 2009. *Quantification de l'amorçage en fissuration d'un contact soumis à des sollicitations en fretting wear*, Rapport de Stage de Master.
- Popov, V. L., 2010. *Contact Mechanics and Friction - Physical Principles and Applications*, Springer-Verlag Berlin Heidelberg.
- Proudhon, H., Basseville, S., 2011. "Finite Element Analysis of Fretting Crack Propagation", *Engineering Fracture Mechanics*, 78, 685-694.
- Stephens, R.I, Fatemi, A., Stephens, R.R., Fuchs, H. O., 2001. *Metal Fatigue in Engineering*, John Wiley & Sons Inc..

Patrícia Rocha Maia, Luiz Carlos Rolim Lopes
Study Of Local Stress State And Fretting Parameters In A Sphere-Plan Contact Under Fretting Fatigue Conditions

Thomson, D., 1998. The national High Cycle Fatigue (HCF) program. In W.A. Strange, ed., 3rd Nat. *Turbine Engine High Cycle Fatigue conference* – Saint Antonio (TX).
Vingsbo, O., Söderberg S., 1988. “On Fretting Maps”, In *Wear* 126, 131–47.

6. RESPONSIBILITY NOTICE

The authors are the only responsible for the printed material included in this paper.